Applied Surface Science 523 (2020) 146483

Contents lists available at ScienceDirect

Applied Surface Science

journal homepage: www.elsevier.com/locate/apsusc

Electronic and photocatalytic performance of boron phosphide-blue phosphorene vdW heterostructures

Ismail Shahid[a], Sheraz Ahmad[a], Nasir Shehzad[b], Sai Yao[a], Chuong V. Nguyen[c], Lixin Zhang[b], Zhen Zhou[a,*]

[a] School of Materials Science and Engineering, Computational Centre for Molecular Science, Institute of New Energy Material Chemistry, Nankai University, Tianjin 300350, PR China
[b] School of Physics, Nankai University, Tianjin 300071, PR China
[c] Department of Materials Science and Engineering, Le Quy Don Technical University, Hanoi 100000, Viet Nam

ARTICLE INFO

Keywords:
Photocatalysis
Heterostructures
Water splitting
First-principles computations
2D materials
Optical properties

ABSTRACT

Hydrogen generation via photocatalytic water splitting is considered as a source of clean energy and an alternative approach to deal with energy crises and environmental problems. By using first-principles computations, we determine that boron phosphide-blue phosphorene van der Waals heterostructure is a potential candidate for overall water splitting at low pH values (0–3). The heterostructure is a semiconductor with a direct band gap of 1.47 eV and possesses type-II band alignment. More importantly, this heterostructure contents the water reduction and oxidation levels for water splitting, with enhanced optical absorption in infrared, visible and ultraviolet regions. Particularly, tensile strain can enhance the optical absorption in the visible range and increase the solar energy conversion efficiency. Our study widens the application of boron phosphide-blue phosphorene heterostructures, and helps design more heterostructured photocatalysts.

1. Introduction

With successive environmental issues and depletion of natural fuels, the scientific community enforces to look for more effective and renewable green energy resources [1]. Photocatalytic water splitting is a good way to produce hydrogen which is sustainable and clean [2]. Among all natural fuels, hydrogen has the highest energy per mass ratio, is the most earth abundant and would not produce toxic substances for environment after burning [3,4]. The key challenging task is to develop highly efficient photocatalysts that endure the properties such as high stability, appropriate band gap and edge positions for straddling the redox potential of water (mainly 1.23 eV band gap is required), absorption of visible solar spectrum, low hole-electron pair recombination, fast charge transfer, and low toxicity and cost. Once the aforementioned requirements are satisfied, photocatalysts can be able to separate water into O_2 and H_2 in an elemental measurement of 2 vs. 1 without consuming any other external agents [5–7]. Up to now, many attempts have been devoted to search for efficient photocatalyst candidates. It has been reported that some two-dimensional (2D) semiconductors are expected to be suitable for photocatalytic water splitting [8,9]. However, not all 2D materials are good for photocatalysis. For instance, large band gaps in ZnO, Fe_2O_3, g-C_3N_4, TiO_2 and CdS limits the absorption of visible light and further reduce their photocatalytic activity [10–12]. In addition, the photocatalytic performance in such materials is poor because the band edge positions are very far away from redox potentials for photocatalytic water splitting [13].

Recently, among 2D monolayers, blue phosphorene (BlueP) has been successfully synthesized [14]. Different from black phosphorene, BlueP is a wide and indirect band gap semiconductor, and the band gap can further be modified in a wide range by applying strain and electric field [15,16]. There have been tight binding (TB) and density functional theory (DFT) computations on electronic properties of BlueP monolayer [15,17–20] and BlueP-based heterostructures [21,22]. 2D boron phosphide (BP) is also reported as a candidate for electronic application. BP has a direct band gap and further its electronic properties can be changed by changing the stacking patterns and external fields [23,24]. BP is found to have a small lattice mismatch and share crystal structure similar to BlueP, making them favourable for the growth of BP-BlueP heterostructures in laboratory [16,25].

Many researchers have studied vertically stacked van der Waals (vdW) heterostructures computationally and even experimentally, which were used to create modern optoelectronic and electronic devices with innovative physical properties and distinct functions [26–33]. Specially, type-II band alignment in heterostructures is

* Corresponding author.
E-mail address: zhouzhen@nankai.edu.cn (Z. Zhou).

https://doi.org/10.1016/j.apsusc.2020.146483
Received 22 January 2020; Received in revised form 14 March 2020; Accepted 14 April 2020
Available online 28 April 2020
0169-4332/

Table 1
The calculated ground-state properties of the monolayers and their heterostructures: lattice parameters of primitive unit cell, bond lengths, interlayer distances (d_0), binding energies (E_b) and bandgaps calculated within PBE and HSE06 functional.

Structures	a (Å)	$d_{(P-P)}$ (Å)	$d_{(B-P)}$ (Å)	d_0 (Å)	E_b (eV)	E_g^{PBE} (eV)	E_g^{HSE} (eV)
BP	3.21	–	1.85	–	–	0.88	1.31
BlueP	3.29	2.26	–	–	–	1.87	2.70
Stacking (AA)	3.24	2.244	1.876	3.101	−0.448	1.00	1.47
Stacking (AB_P)	3.25	2.244	1.876	3.103	−0.431	0.76	1.19
Stacking (AB_B)	3.25	2.244	1.876	3.103	−0.416	1.03	1.50

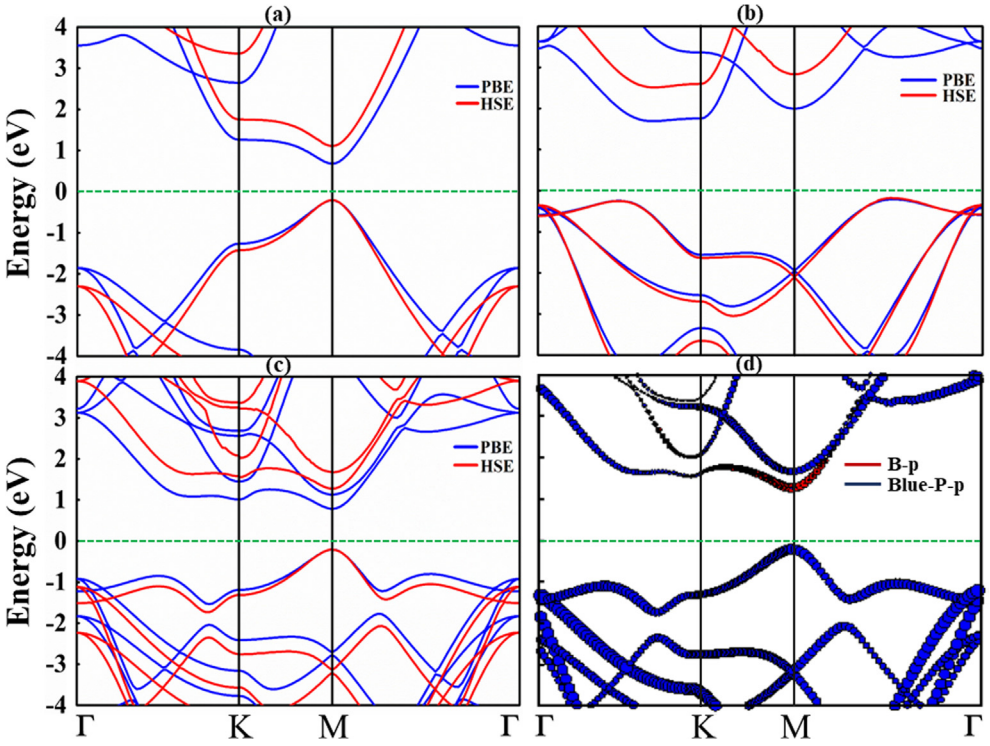

Fig. 1. Calculated electronic structures of (a) monolayer BP (b) monolayer BlueP (c) BP-BlueP heterostructure with PBE (blue) and HSE06 (red) functionals. (d) Weighted band structure of BP-BlueP heterostructure. (For interpretation of the references to colour in this figure legend, the reader is referred to the web version of this article.)

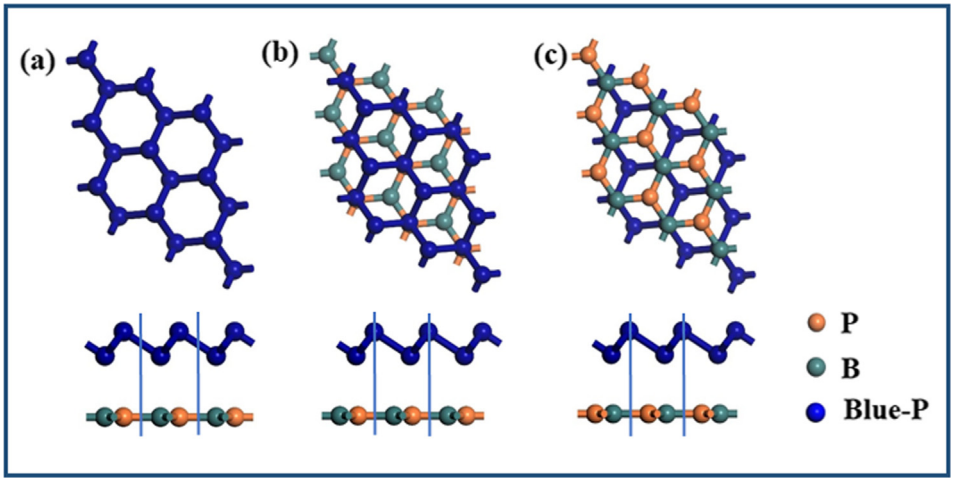

Fig. 2. Optimised top (upper panel) and side (lower panel) views of three different stackings of BP-BlueP heterostructure (a-c). The unit cell is identified by vertical blue lines.

beneficial for the detection and harvesting of light. This kind of band alignment significantly slows down the electron-hole pair recombination, which is extremely required for photovoltaic and photocatalytic devices [34–37]. Recently, various BlueP-based heterostructures have been studied, such as BlueP-BSe [38], BlueP-AlN [39], BlueP-MXenes [22] and BlueP-TMDCs [36]. Therefore, it is attractive to check whether BP and BlueP can form a stable 2D hybrid vdW heterostructure to achieve superior electronic and photocatalytic performances. To discuss the aforementioned goals, we computationally explored the electronic properties, band edge positions, charge transfer, strain effect and optical performance of BP-BlueP vdW heterostructures by using first-principles computations. Our results reveal that BP-BlueP

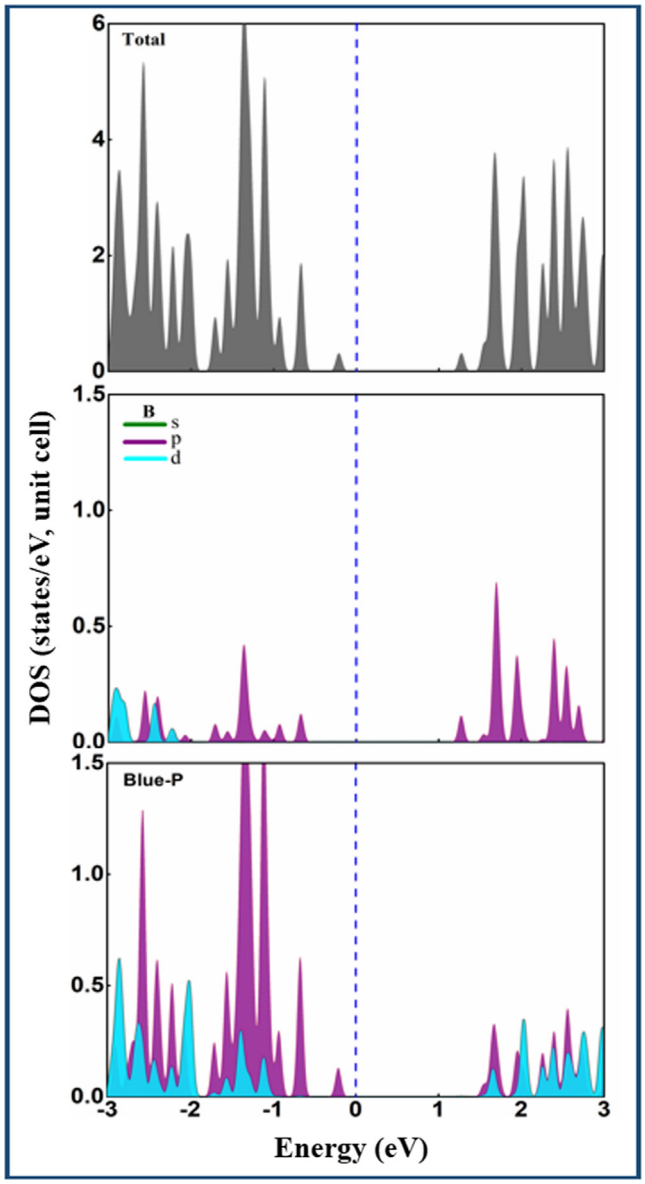

Fig. 3. Total (TDOS) and partial density of states (PDOS) of most favourable AA-stacking of BP-BlueP heterostructure.

heterostructures are favourable candidates for photocatalytic water splitting.

2. Computational

All DFT computations were performed within Vienna ab initio simulation package (VASP) [40]. The projected augmented wave [41] method and generalized gradient approximation (GGA) functional of Perdew, Burke, and Ernzerhof (PBE) were used to optimize the geometric structure [42]. HSE06 functional was employed to obtain more precise electronic structures [43], as well as Grimme's D2 correction to describe weak vdW interactions between adjacent layers [44]. A 25 Å vacuum was used along z direction to avoid the periodic images. Cut-off energy of 500 eV and k-meshes of 6 × 6 × 1 were used for structural relaxation. For fully relaxed structures the convergence criteria for force and energy were set to 0.01 eVÅ^{-1} and 10^{-5} eV, respectively. Phonon spectrum calculations were conducted with PHONOPHY code [45]. Ab-initio molecular dynamics (AIMD) simulations were performed at 500 K with a time step of 2.0 fs for 10 ps, which was controlled by a Nose-Hoover thermostat [46,47].

3. Results and discussion

First, we studied the geometric structures of pristine BP and BlueP monolayers which are depicted in Fig. S1. BP shows a planer honeycomb lattice with an optimized lattice constant of 3.21 Å, which is consistent with earlier work [21]. The bond length between B and P is about 1.85 Å. BlueP has also honeycomb buckled lattice and its optimized lattice constant is 3.29 Å. The bond length between P-P atoms is 2.26 Å (see Table 1). These structural parameters are in good agreement with previous work [38]. The calculated band structures are shown in Fig. 1. The blue and red lines represent PBE and HSE06 results, respectively. It is clear that BP is a direct band gap semiconductor with both the conduction band minimum (CBM) and valence band maximum (VBM) at the M point as shown in Fig. 1(a). The calculated values of band gap for BP with PBE and HSE06 functional are 0.88 and 1.31 eV, respectively. The results are consistent with a previous report [48]. BlueP is an indirect band gap semiconductor with the CBM at the Γ-K path and the VBM at the Γ-M path, as shown in Fig. 1(b). The band gap values are 1.87 and 2.70 eV with PBE and HSE06, respectively. These values are consistent with previous results [38]. Accurate electronic structures are very meaningful for photocatalytic activity; therefore, we adopt HSE06 functional since PBE usually underestimates the band gap.

Then we designed the BP-BlueP heterostructure. Small lattice mismatch (2.43%) between BP and BlueP monolayers makes it feasible in experimental preparation of the heterostructure. Three possible configurations, (a) AA-stacking, (b) AB_P-stacking and (c) AB_B-stacking for the heterostructure, are considered as shown in Fig. 2. In AA stacking both P atoms are on top of B and P atoms while one P atom is on top of P and B, respectively and the other P atom is on top of hexagonal center in AB_P- and AB_B-stacking.

To check the relative stability of different configurations of the heterostructure, we calculated the binding energy by $E_b = E_{BP/BlueP} - E_{BP} - E_{BlueP}$, where $E_{BP/BlueP}$, E_{BP} and E_{BlueP} show the total energies of BP-BlueP heterostructure, BP and BlueP monolayer, respectively. The negative binding energies confirm the stability of given configurations and show stronger interaction between BP and BlueP monolayers. Stacking with large binding energy is considered to be favourable. Further we confirmed the dynamic stability with different stacking patterns of BP-BlueP heterostructure, and the results are depicted in Fig. S2. All phonon modes have no negative frequencies, confirming the dynamic stability of the heterostructure. Furthermore, we performed AIMD simulations at 500 K, as depicted in Fig. S3. The results show that BP-BlueP heterostructures are quite stable. A small fluctuation in energy is due to the transition from AA stacking to AB_B-stacking, which does not affect the electronic properties. The optimized lattice constant, bond length, interlayer distance, binding energy and band gap are summarized in Table 1. Thus, we will consider the most stable stacking (AA) of BP-BlueP heterostructure for further investigations. The AA-stacking BP-BlueP heterostructure shows semiconducting nature with a direct band gap of 1.47 eV in Fig. 1(c), while the band structures of AB_P- and AB_B-stacking are shown in Fig. S4 which exhibit the same nature as AA-stacking. Both the CMB and VBM lie at the M point of the Brillion zone (BZ). The weighted band structure of the AA-stacking heterostructure is depicted in Fig. 1(d). The red and blue colour represent BP and BlueP monolayer, respectively. We can see that the CBM of AA-stacking comes from the BP monolayer, while its VBM is mainly contributed by BlueP monolayer, resulting in the formation of Type-II band alignment at the interface of the heterostructure. Such type of band alignment efficiently separates free electrons and holes, and slows down the electron-hole pair recombination. This phenomenon helps in facilitating solar energy conversion and high efficiency optoelectronics [29,49,50]. Moreover, it is clear that the band gap of this heterostructure is a little larger than 1.23 eV, a critical band gap for photocatalytic water splitting, demonstrating good performance as a visible light photocatalyst [49]. The partial density of states (PDOS) provides more information about the weighted band structure as shown in Fig. 3.

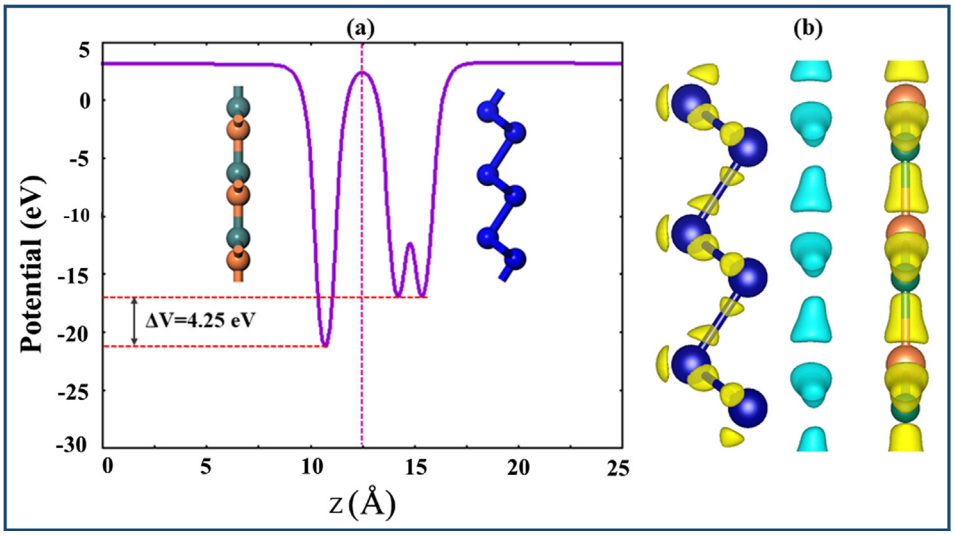

Fig. 4. Electrostatic potential energy (a) and charge density difference of BP-BlueP heterostructure (b).

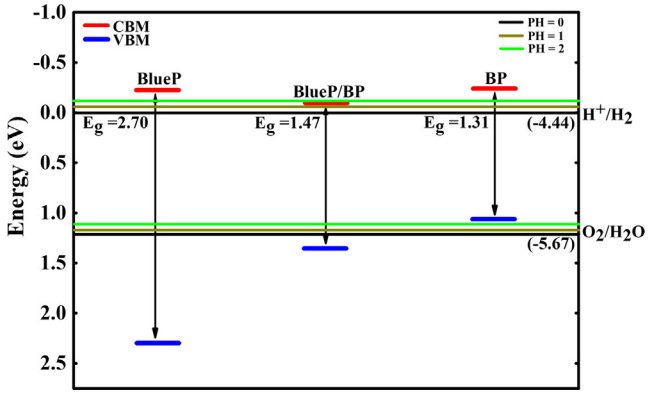

Fig. 5. Band edge positions of BP-BlueP heterostructure and their corresponding monolayers. Water oxidation (O_2/H_2O) and reduction (H^+/H_2) at pH = 0, 1 and 2.

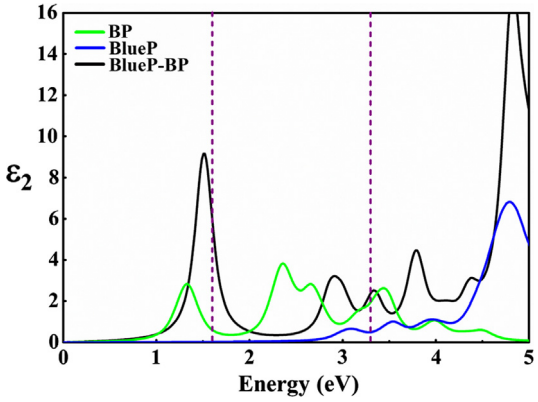

Fig. 6. The calculated imaginary part of dielectric function of BP-BlueP heterostructure and their corresponding monolayers.

The CBM is due to the 3p state of B atoms while the VBM is due to the 3p state of P atoms in BlueP, confirming type-II band alignment.

Charge transfer across the interface of the heterostructure is very important. Moreover, the heterostructure reduces the band gap compared with pristine monolayers due to significant interaction between the monolayers and redistribution of charge in the heterostructure. Therefore, the charge density difference was investigated to show the specific state of charge transfer. Charge density difference is obtained by $\Delta\rho = \rho_{(BP\text{-}BlueP)} - \rho_{(BP)} - \rho_{(BlueP)}$, where $\rho_{(BP\text{-}BlueP)}$, $\rho_{(BP)}$ and $\rho_{(BlueP)}$ are charge density of BP-BlueP heterostructure, pristine BP and BlueP monolayers, respectively, which is depicted in Fig. 4(b). The minimum amount of energy required for removing an electron from the surface is referred to work function (Φ). Precise calculation of Φ can also help establish the direction of charge flow in the surface. The results demonstrate that BlueP monolayer donates electrons to BP monolayer because the work function of BP is larger than that of BlueP (Φ_{BP} = 1.98 eV, Φ_{BlueP} = 0.99 eV). This finding leads to the formation of p-doping in BlueP and n-doping in BP. Furthermore, electrostatic potential along Z-direction is plotted in Fig. 4(a). The BP monolayer has deeper potential than BlueP monolayer showing that electron is forced to drive from BlueP to BP monolayer. The potential energy ($\triangle V$) drops across the monolayers are found to be 4.25 eV.

Our BP-BlueP heterostructure provides an appropriate band gap for overall photocatalytic water splitting. Hence, the photocatalytic response of pristine BP and BlueP monolayers and their vdW heterostructure was checked by using Mulliken electronegativity in $E_{VBM} = \chi - E_{elec\text{-}p} + 1/2E_g$ and $E_{CBM} = E_{VBM} - E_g$ [51,52], where E_{VBM} and E_{CBM} are valence and conduction band edge potential, respectively, χ shows geometric mean of Mulliken electronegativity of isolated atoms, E_g is the band gap value, and $E_{elec\text{-}p}$ is the standard electrode potential on hydrogen scale whose value is -4.5 eV. The band edge positions with respect to water redox potentials are depicted in Fig. 5 for pristine monolayers and their heterostructure. The calculated band edge position in this work for BlueP is consistent with earlier work [38,39]. The VBM and CBM of BlueP is higher than those of BP, further confirming type-II band alignment in BP-BlueP heterostructure, which potentially enhances the photocatalytic performance. The band edges of BP-BlueP heterostructure locate at energetically favourable positions, representing that BP-BlueP heterostructure is able to split water in acidic solutions (pH = 0–2). The pristine BP monolayer is capable to dissociate water into H^+/H_2 but fails to oxidize water into O_2/H_2O, while BlueP has favourable band edge positions for water splitting at pH = 0 but its band gap is larger than 2.20 eV, making it unfavourable for absorbing wide solar spectrum, which reduces their potential conversion efficiency [49,53,54].

To explain this issue we calculated the imaginary part (ε_2) of dielectric function of pristine BP and BlueP monolayers along with their BP-BlueP heterostructure as shown in Fig. 6. As we know that infrared, visible and ultraviolet light account for about 43%, 50% and 7% of the solar energy [55]. The first peak of BP originates in low energy range (infrared region) due to smaller band gap and further covers a long range of visible spectrum, while BlueP shows good absorption in both

visible and ultraviolet region. More interestingly, BP-BlueP heterostructure can absorb in near infrared, visible and ultraviolet region, meaning that BP-BlueP heterostructure covers large portion of the solar energy. The photocatalytic performance of our BP-BlueP heterostructure is superior to that of some reported BlueP-based and other heterostructures [38,39,56]. Thus, the BP-BlueP heterostructure can be consider as a promising candidate for photovoltaic devices and photocatalysts.

Strain engineering is an effective technique to tune the properties of 2D materials [57]. Here we will discuss the influence of strain on band gaps and band edge positions of vdW BP-BlueP heterostructure. The inner layer strain (ε) is defined as $\varepsilon = (a - a_0)/a_0$, where a and a_0 are the lattice parameters of strained and unstrained system, respectively. All strains are applied within elastic limit, which are completely reversible. The band gaps smoothly increase and decrease by applying tensile and compression strain, respectively, as shown in Figs. S5 and S6. We can observe that small strains not only decrease the bandgaps but also keep both the CBM and VBM at appropriate energy levels for photocatalytic water splitting as shown in Fig. S7. Furthermore, transition from type-II to type-I band alignment occurs in compression strain. Usually, type-I band alignment is associated with fast rate of recombination which is unfavourable for photocatalysis [58]. Therefore, this type of band alignment can be utilized in optoelectronic devices due to the fast electron-hole pair recombination [59]. More interestingly, the tensile strain shifts the optical peaks towards higher energy, which enhances the optical absorption in visible spectrum. The optical absorption of BP-BlueP heterostructure is superior in visible spectrum at 4% tensile strain, which is illustrated in Fig. S8. Most reduction/oxidation reactions occur in aqueous solutions. We used the pH dependent reduction (-4.44 eV + pH $\times$ 0.059 eV) and oxidation (-5.67 eV + pH $\times$ 0.059 eV) [53]. To consider the effect of pH on water splitting, we compare the redox potentials with pH = 0, 1, 2 and 3. The results are depicted in Fig. S7. We can see that the band edge positions of BP-BlueP heterostructure still straddle the redox potential of water even at pH = 3, which conclude that vdW BP-BlueP heterostructure could be a favourable candidate for photocatalytic overall water splitting.

Here we also checked the effect of H_2, H_2O and O_2 adsorb on perfect and defected BP-BlueP heterostructures. Similar to phosphorene monolayers [60,61], O_2 chemically adsorbs on the BlueP surface with little effect on the stability and electronic properties of heterostructures, and dissociates at the BlueP surface with vacancies, while H_2 and H_2O have no effect on the stability and electronic properties of heterostructures as shown in Figs. S9-S15. Therefore, O_2 would degrade the heterostructures with defects, which should be avoided as water splitting photocatalysts.

4. Conclusions

We have investigated the electronic and photocatalytic properties of BP-BlueP vdW heterostructures by using first-principles computations. Our heterostructures exhibit dynamic and thermal stability and high experimental feasibility. We found that BP-BlueP heterostructure is a direct band semiconductor with type-II band alignment. In addition, the VBM and CBM edges of BP-BlueP heterostructure straddle the standard redox potentials for water splitting and are useful for dissociating water into H_2 and O_2 at low pH values. More interestingly, BP-BlueP heterostructure harvests the solar spectrum in infrared, visible and ultraviolet light zones. Strain is an effective technique to tune the properties of BP-BlueP heterostructure. We confirmed that band gaps, band edges positions and optical absorption of BP-BlueP heterostructure could be tailored by tensile and compression strain. Tensile strain enhances the optical absorption in visible range, which increases the solar energy conversion efficiency. Our results indicate that BP-BlueP vdW heterostructure can be a potential photocatalyst for overall water splitting.

CRediT authorship contribution statement

Ismail Shahid: Conceptualization, Methodology, Data curation, Writing - original draft. **Sheraz Ahmad:** Writing - review & editing. **Nasir Shehzad:** Writing - review & editing. Sai Yao**:** Writing - review & editing. **Chuong V. Nguyen:** Writing - review & editing. **Lixin Zhang:** Writing - review & editing. **Zhen Zhou:** Supervision, Writing - review & editing.

Acknowledgements

This work was supported by National Natural Science Foundation of China (11574157).

Author's contributions

Ismail Shahid wrote the main manuscript. Sheraz Ahmad, Nasir shehzad, Sai Yao, Chuong V. Nguyen and Lixin Zhang reviewed the manuscript. Zhen Zhou supervised the project.

Declaration of Competing Interest

There are no conflicts of interest to declare.

Appendix A. Supplementary material

Supplementary data to this article can be found online at https://doi.org/10.1016/j.apsusc.2020.146483.

References

[1] M.S. Dresselhaus, I.L. Thomas, Alternative energy technologies, Nature 414 (2001) 332–337.
[2] A. Fujishima, K. Honda, Electrochemical photolysis of water at a semiconductor electrode, Nature 238 (1972) 37–38.
[3] J.A. Turner, Science 305 (2013) 972–974.
[4] A. Banerjee, Materials Modelling for energy harvesting: from conversion to application through storage, Acta Univ. Upsaliensis (2019).
[5] G. Zhang, Z.A. Lan, L. Lin, S. Lin, X. Wang, Overall water splitting by Pt/gC_3N_4 photocatalysts without using sacrificial agents, Chem. Sci. 7 (2016) 3062–3066.
[6] B. Bhanvase, T. Shende, S. Sonawane, A review on graphene-TiO_2 and doped graphene-TiO_2 nanocomposite photocatalyst for water and wastewater treatment, Environ. Technol. Rev. 6 (2017) 1–14.
[7] J. Schneider, D. Bahnemann, Undesired role of sacrificial reagents in photocatalysis, J. Phys. Chem. Lett. 4 (2013) 3479–3483.
[8] S. Yao, X. Zhang, Z. Zhang, A. Chen, Z. Zhou, 2D Triphosphides: SbP_3 and GaP_3 monolayer as promising photocatalysts for water splitting, Int. J. Hydrogen Energy 44 (2019) 5948–5954.
[9] M. Idrees, H. Din, R. Ali, G. Rehman, T. Hussain, C. Nguyen, I. Ahmad, B. Amin, Optoelectronic and solar cell applications of Janus monolayers and their van der Waals heterostructures, PCCP 21 (2019) 18612–18621.
[10] S. Zhang, B. Peng, S. Yang, H. Wang, H. Yu, Y. Fang, F. Peng, Non-noble metal copper nanoparticles-decorated TiO_2 nanotube arrays with plasmon-enhanced photocatalytic hydrogen evolution under visible light, Int. J. Hydrogen Energy 40 (2015) 303–310.
[11] X. Zhang, W. An, Y. Li, J. Hu, H. Gao, W. Cui, Efficient photo-catalytic hydrogen production performance and stability of a three-dimensional porous CdS NPs-graphene hydrogel, Int. J. Hydrogen Energy 43 (2018) 9902–9913.
[12] R. Pawar, C.S. Lee, Heterogeneous Nanocomposite-Photocatalysis for Water Purification, Elsevier Science, 2015.
[13] W. Hu, L. Lin, R. Zhang, C. Yang, J. Yang, Highly efficient photocatalytic water splitting over edge-modified phosphorene nanoribbons, J. Am. Chem. Soc. 139 (2017) 15429–15436.
[14] J.L. Zhang, S. Zhao, C. Han, Z. Wang, S. Zhong, S. Sun, R. Guo, X. Zhou, C.D. Gu, K.D. Yuan, Epitaxial growth of single layer blue phosphorus: a new phase of two-dimensional phosphorus, NANO Lett. 16 (2016) 4903–4908.
[15] B. Ghosh, S. Nahas, S. Bhowmick, A. Agarwal, Electric field induced gap modification in ultrathin blue phosphorus, Phys. Rev. B 91 (2015) 115433.
[16] Z. Zhu, D. Tománek, Semiconducting layered blue phosphorus: a computational study, Phys. Rev. Lett. 112 (2014) 176802.
[17] Y. Aierken, D. Çakır, C. Sevik, F.M. Peeters, Thermal properties of black and blue phosphorenes from a first-principles quasiharmonic approach, Phys. Rev. B 92 (2015) 081408.
[18] Y. Ding, Y. Wang, Structural, electronic, and magnetic properties of adatom adsorptions on black and blue phosphorene: a first-principles study, J. Phys. Chem. C 119 (2015) 10610–10622.

[19] M. Sun, W. Tang, Q. Ren, S.K. Wang, J. Yu, Y. Du, A first-principles study of light non-metallic atom substituted blue phosphorene, Appl. Surf. Sci. 356 (2015) 110–114.
[20] Y. Mogulkoc, M. Modarresi, A. Mogulkoc, Y. Ciftci, Electronic and optical properties of bilayer blue phosphorus, Comput. Mater. Sci. 124 (2016) 23–29.
[21] Y. Mogulkoc, M. Modarresi, A. Mogulkoc, B. Alkan, Electronic and optical properties of boron phosphide/blue phosphorus heterostructures, PCCP 20 (2018) 12053–12060.
[22] G. Rehman, S. Ali Khan, R. Ali, I. Ahmad, L.Y. Gan, B. Amin, Van der Waals heterostructures of blue phosphorene and scandium-based MXenes monolayers, J. Appl. Phys., 126 (2019) 143101.
[23] H. Şahin, S. Cahangirov, M. Topsakal, E. Bekaroglu, E. Akturk, R.T. Senger, S. Ciraci, Monolayer honeycomb structures of group-IV elements and III-V binary compounds: first-principles calculations, Phys. Rev. B 80 (2009) 155453.
[24] X. Chen, C. Tan, Q. Yang, R. Meng, Q. Liang, J. Jiang, X. Sun, D. Yang, T. Ren, Effect of multilayer structure, stacking order and external electric field on the electrical properties of few-layer boron-phosphide, PCCP 18 (2016) 16229–16236.
[25] S. Demirci, N. Avazlı, E. Durgun, S. Cahangirov, Structural and electronic properties of monolayer group III monochalcogenides, Phys. Rev. B 95 (2017) 115409.
[26] Z.S. Wu, Y. Zheng, S. Zheng, S. Wang, C. Sun, K. Parvez, T. Ikeda, X. Bao, K. Müllen, X. Feng, Stacked-layer heterostructure films of 2D thiophene nanosheets and graphene for high-rate all-solid-state pseudocapacitors with enhanced volumetric capacitance, Adv. Mater. 29 (2017) 1602960.
[27] M. Long, E. Liu, P. Wang, A. Gao, H. Xia, W. Luo, B. Wang, J. Zeng, Y. Fu, K. Xu, Broadband photovoltaic detectors based on an atomically thin heterostructure, NANO Lett. 16 (2016) 2254–2259.
[28] X.H. Li, B.J. Wang, X.L. Cai, L.W. Zhang, G.D. Wang, S.H. Ke, Tunable electronic properties of arsenene/GaS van der Waals heterostructures, RSC Adv. 7 (2017) 28393–28398.
[29] X.H. Li, B.J. Wang, X.L. Cai, W.Y. Yu, L.W. Zhang, G.D. Wang, S.H. Ke, Arsenene/Ca$(OH)_2$ van der Waals heterostructure: Strain tunable electronic and photocatalytic properties, RSC Adv. 7 (2017) 44394–44400.
[30] Q. Zhang, X. Xiao, R. Zhao, D. Lv, G. Xu, Z. Lu, L. Sun, S. Lin, X. Gao, J. Zhou, Two-dimensional layered heterostructures synthesized from core-shell nanowires, Angew. Chem. Int. Ed. 54 (2015) 8957–8960.
[31] Z. Cui, K. Ren, Y. Zhao, X. Wang, H. Shu, J. Yu, W. Tang, M. Sun, Electronic and optical properties of van der Waals heterostructures of g-GaN and transition metal dichalcogenides, Appl. Surf. Sci. 492 (2019) 513–519.
[32] K. Ren, Y. Luo, S. Wang, J.P. Chou, J. Yu, W. Tang, M. Sun, A van der Waals heterostructure based on graphene-like gallium nitride and boron selenide: a high-efficiency photocatalyst for water splitting, ACS Omega 4 (2019) 21689–21697.
[33] K. Ren, J. Yu, W. Tang, A two-dimensional vertical van der Waals heterostructure based on g-GaN and $Mg(OH)_2$ used as a promising photocatalyst for water splitting: a first-principles calculation, J. Appl. Phys. 126 (2019) 065701.
[34] J. Kang, S. Tongay, J. Zhou, J. Li, J. Wu, Band offsets and heterostructures of two-dimensional semiconductors, Appl. Phys. Lett. 102 (2013) 012111.
[35] X.L. Wei, H. Zhang, G.C. Guo, X.B. Li, W.M. Lau, L.M. Liu, Modulating the atomic and electronic structures through alloying and heterostructure of single-layer MoS_2, J. Mater. Chem. A 2 (2014) 2101–2109.
[36] Q. Peng, Z. Wang, B. Sa, B. Wu, Z. Sun, Electronic structures and enhanced optical properties of blue phosphorene/transition metal dichalcogenides van der Waals heterostructures, Sci. Rep. 6 (2016) 31994.
[37] V.O. Özcelik, J.G. Azadani, C. Yang, S.J. Koester, T. Low, Band alignment of two-dimensional semiconductors for designing heterostructures with momentum space matching, Phys. Rev. B 94 (2016) 035125.
[38] B.J. Wang, X.H. Li, R. Zhao, X.L. Cai, W.Y. Yu, W.B. Li, Z.S. Liu, L.W. Zhang, S.H. Ke, Electronic structures and enhanced photocatalytic properties of blue phosphorene/BSe van der Waals heterostructures, J. Mater. Chem. A 6 (2018) 8923–8929.
[39] Q. Yang, C.J. Tan, R.S. Meng, J.K. Jiang, Q.H. Liang, X. Sun, D.G. Yang, X.P. Chen, AlN/BP heterostructure photocatalyst for water splitting, IEEE Electron Dev. Lett. 38 (2016) 145–148.
[40] G. Kresse, J. Hafner, Ab initio molecular dynamics for liquid metals, Phys. Rev. B 47 (1993) 558.
[41] P.E. Blöchl, Projector augmented-wave method, Phys. Rev. B 50 (1994) 17953.
[42] J. Perdew, K. Burke, M. Ernzerhof, Generalized gradient approximation made simple, Phys. Rev. Lett. 77 (1996) 3865–3868.
[43] J. Paier, M. Marsman, K. Hummer, G. Kresse, I.C. Gerber, J.G. Ángyán, Screened hybrid density functionals applied to solids, J. Chem. Phys. 124 (2006) 154709.
[44] S. Grimme, Semiempirical GGA-type density functional constructed with a long-range dispersion correction, J. Comput. Chem. 27 (2006) 1787–1799.
[45] A. Togo, I. Tanaka, First principles phonon calculations in materials science, Scripta Mater. 108 (2015) 1–5.
[46] W.G. Hoover, Canonical dynamics: Equilibrium phase-space distributions, Phys. Rev. A 31 (1985) 1695.
[47] S. Nosé, A unified formulation of the constant temperature molecular dynamics methods, J. Chem. Phys. 81 (1984) 511–519.
[48] A. Mogulkoc, Y. Mogulkoc, M. Modarresi, B. Alkan, Electronic structure and optical properties of novel monolayer gallium nitride and boron phosphide heterobilayers, PCCP 20 (2018) 28124–28134.
[49] Y. Li, Y.L. Li, B. Sa, R. Ahuja, Review of two-dimensional materials for photocatalytic water splitting from a theoretical perspective, Catal. Sci. Technol. 7 (2017) 545–559.
[50] J. Liao, B. Sa, J. Zhou, R. Ahuja, Z. Sun, Design of high-efficiency visible-light photocatalysts for water splitting: MoS2/AlN (GaN) heterostructures, J. Phys. Chem. C 118 (2014) 17594–17599.
[51] J. Liu, X. Fu, S. Chen, Y. Zhu, Electronic structure and optical properties of Ag_3PO_4 photocatalyst calculated by hybrid density functional method, Appl. Phys. Lett. 99 (2011) 191903.
[52] H.L. Zhuang, R.G. Hennig, Theoretical perspective of photocatalytic properties of single-layer SnS_2, Phys. Rev. B 88 (2013) 115314.
[53] H.L. Zhuang, R.G. Hennig, Single-layer group-III monochalcogenide photocatalysts for water splitting, Chem. Mater. 25 (2013) 3232–3238.
[54] A.J. Bard, M.A. Fox, Artificial photosynthesis: solar splitting of water to hydrogen and oxygen, Acc. Chem. Res. 28 (1995) 141–145.
[55] R. Peng, Y. Ma, B. Huang, Y. Dai, Two-dimensional Janus PtSSe for photocatalytic water splitting under the visible or infrared light, J. Mater. Chem. A 7 (2019) 603–610.
[56] H. Din, M. Idrees, A. Albar, M. Shafiq, I. Ahmad, C.V. Nguyen, B. Amin, Rashba spin splitting and photocatalytic properties of GeC− M SSe (M= Mo, W) van der Waals heterostructures, Phys. Rev. B 100 (2019) 165425.
[57] B. Amin, T.P. Kaloni, U. Schwingenschlögl, Strain engineering of WS_2, WSe_2, and WTe_2, RSC Adv. 4 (2014) 34561–34565.
[58] Z. Cheng, F. Wang, T.A. Shifa, C. Jiang, Q. Liu, J. He, Efficient photocatalytic hydrogen evolution via band alignment tailoring: controllable transition from Type-I to Type-II, Small 13 (2017) 1702163.
[59] Z. Lu, D. Lockwood, J.-M. Baribeau, Quantum confinement and light emission in SiO_2/Si superlattices, Nature 378 (1995) 258.
[60] A. Kistanov, Y. Cai, K. Zhou, S. Dmitriev, Y.W. Zhang, The Role of H_2O and O_2 Molecules and Phosphorus Vacancies in the Structure Instability of Phosphorene, 2D Materials 4 (2017) 015010.
[61] N. Liu, S. Zhou, Gas adsorption on monolayer blue phosphorus: implications for environmental stability and gas sensors, Nanotechnology 28 (2017) 175708.